Push-pull mechanics of E-cadherin ectodomains in biomimetic adhesions

Kartikeya Nagendra[1, 2], Adrien Izzet[1], Nicolas Byron Judd[1], Ruben Zakine[1], Leah Friedman[1,3], Oliver J Harrison[4], Léa-Laetitia Pontani[5], Lawrence Shapiro[4, 6], Barry Honig[4, 6, 7, 8], and Jasna Brujic[1, 9*]

[1]Center for Soft Matter Research, Department of Physics, New York University, New York, NY 10003
[2]Molecular Biophysics and Biochemistry Training Program, NYU Grossman School of Medicine, New York, NY 10016
[3]Département de Physique, École Normale Supérieure, PSL University, 75005 Paris, France
[4]Department of Biochemistry and Molecular Biophysics, Columbia University, New York, NY 10032, USA
[5]Laboratoire Jean Perrin, Institut de Biologie Paris-Seine, Sorbonne Université, CNRS, F-75005 Paris, France
[6]Zuckerman Mind Brain Behavior Institute, Columbia University, New York, NY 10027, USA
[7]Department of Medicine, Division of Nephrology, Columbia University, New York, NY 10032, USA
[8]Department of Systems Biology, Columbia University, New York, NY 10032, USA
[9]Laboratoire de Physique et Mécanique de Milieux Hétérogènes, UMR 7636, CNRS, ESPCI Paris-PSL, Sorbonne Université, Université Paris Cité, 75005 Paris, France

E-cadherin plays a central role in cell-cell adhesion. The ectodomains of wild type cadherins form a crystalline-like two dimensional lattice in cell-cell interfaces mediated by both *trans* (apposed cell) and *cis* (same cell) interactions. In addition to these extracellular forces, adhesive strength is further regulated by cytosolic phenomena involving α and β–catenin–mediated interactions between cadherin and the actin cytoskeleton. Cell-cell adhesion can be further strengthened under tension through mechanisms that have not been definitively characterized in molecular detail. Here we quantitatively determine the role of the cadherin ectodomain in mechanosensing. To this end, we devise an E-cadherin-coated emulsion system, in which droplet surface tension is balanced by protein binding strength to give rise to stable areas of adhesion. To reach the honeycomb/cohesive limit, an initial emulsion compression by centrifugation facilitates E-cadherin *trans*-binding, while a high protein surface concentration enables the *cis*-enhanced stabilization of the interface. We observe an abrupt concentration dependence on recruitment into adhesions of constant crystalline density, reminiscent of a first-order phase transition. Removing the lateral *cis*-interaction with a "*cis* mutant" shifts this transition to higher surface densities leading to denser, yet weaker adhesions. In both proteins, the stabilization of progressively larger areas of deformation is consistent with single-molecule experiments that show a force-dependent lifetime enhancement in the cadherin ectodomain, which may be attributed to the "X-dimer" bond.

Correspondence: ***jb2929@nyu.edu***

Significance

The cytoskeletal role in reinforcing cell-cell adhesion is well known, but the contribution of the extracellular E-cadherin domains remains elusive. This work uses a biomimetic emulsion system to demonstrate the strengthening and recruitment of E-cadherin ectodomains in response to push-pull mechanics. We find that E-cadherin adhesion areas grow linearly with the number of molecules, indicative of a constant protein density. Moreover, we observe abrupt recruitment into crystalline adhesions as a function of surface concentration, consistent with the proposal of a first-order phase transition at adhesion junctions. Our system is compatible with biological cells, opening the field to biophysical studies of the hybrid system.

Introduction

E-cadherin adhesion plays a crucial role in mechanical processes in biology, such as morphogenesis, development (1–3), maintenance of tissue structure (4–7) and tumor metastasis (8, 9). *In-vivo*, cadherins form cell-cell junctions through the cooperative action of *trans* and *cis* binding (10, 11). Extracellular *trans* dimers undergo a homophilic interaction with a free energy of binding that has been measured *in vitro* to be in the range of $9-10\mathrm{k_BT}$ (12) in 3-D bulk solution. These dimers laterally cluster via *cis* interactions on the cell surface into a 2D lattice at adhesion sites, with a 2D binding energy predicted to be on the order of $4\ \mathrm{k_BT}$ by numerical simulations (13). The clustering of cadherins at adherens junctions is driven by both intra- and extracellular interactions (14–16).

There is increasing evidence that cadherin adhesions are active mechanical sensors (17–23). More specifically, intracellular domains interact with the actin cytoskeleton through adaptor proteins, α and β catenin, which have been shown to be tension-dependent (24–26). Whether the mechanosensitive behavior of E-cadherin is due to its intrinsic molecular properties or due to those of the cadherin cytoskeletal complex is unclear. Of note, extracellular cadherin domains have been shown to exhibit mechanosensitive catch-bond properties in single-molecule force-spectroscopy experiments (27–29).

Simplified systems of cadherin-functionalized emulsions, liposomes, and model membranes, have served as useful probes of the mechanisms underlying *cis* and *trans* cooperativity (30–35). Nevertheless, the mechanosensing effects of extracellular cadherin adhesion and the relative contribution of *cis* and *trans* binding have not been quantified. Here, we investigate extracellular cadherin adhesion in a tissue-mimetic emulsion, where compression and relaxation, protein surface concentration, and the presence of *cis* interactions can be independently controlled.

Using emulsions, we mimic this cellular adherens junction formation by pushing the emulsions together through a calibrated pressure in the kPa range to facilitate protein recruit-

ment and adhesion (36). This applied pressure mimics the protrusive pushing forces driven by the actin-based Arp2/3 complex, which are known to be necessary for cells to efficiently form and extend cadherin adhesions (37). After compression by centrifugation, the emulsion is allowed to relax back to mechanical equilibrium, in which there is a balance between surface tension and the adhesive energy of protein binding. This step aims to mimic the stabilization of adhesion by cellular pulling forces (38). The resulting droplet deformation allows us to estimate the average binding energy per cadherin dimer. Comparing wild type (WT) and *cis*-deficient mutant (MT) shows that *cis* interactions significantly contribute to the stabilization of adhesions and lead to larger areas of deformation (10).

For both WT and MT, we find a pressure-sensitive adhesion response. The larger the applied pressure and therefore droplet strain, the larger the equilibrium adhesion size. At the maximum pressure, we reach the honeycomb limit and study the effect of cadherin surface concentration. The WT self-assembles into adhesions with a constant density of 15.7×10^3 cadherins$/^2$ independent of initial concentration. This finding is consistent with numerical simulations that propose that *cis* interactions drive crystallization in cadherin adhesion in 2-D (13, 39). The absence of *cis* interactions allows the MT to freely rearrange until it reaches a jamming density of 20.1×10^3 cadherins$/^2$, which is higher than that of the WT crystal. The solid nature of these adhesions in both WT and MT is confirmed by fluorescence recovery after photobleaching (FRAP) measurements.

Interestingly, we observe that a wide range of adhesion areas can be stabilized by a constant cadherin density, which we interpret via a tension-dependent binding free energy of cadherin dimers. Our experiments indicate that the binding energy progressively increases with droplet strain, offering a scale of binding energies from 1.6 $\mathrm{k_BT}$ in the weak-binding regime, up to 20 $\mathrm{k_BT}$ per molecule at the cohesive limit. Our results suggest an intrinsic bond strengthening due to applied tension, suggesting that E-cadherin mechanosensitivity is due in part to intrinsic molecular properties of E-cadherin.

Results

Our biomimetic emulsion system mimics the outer cell membrane, but replaces the cytoskeleton with silicone oil, as shown in Fig. 1A. The oil-in-water interface has a surface tension of $7\mathrm{mN/m}$ in Fig. S2 A and B. The monolayer membrane is stabilized by a mixture of SDS, Egg-PC (EPC), and DGS-NTA-Ni phospholipids, which serve to functionalize the droplets with E-cadherin (30, 41).

The cost of lipid desorption has been estimated to be between $32 - 40k_BT$ (42), beyond the scope of E-cadherin binding energies. This indicates that the cost of lipid desorption is much higher than protein rupture.

Droplets are generated using microfluidics, which gives rise to monodisperse ($D = 20 \pm 1$) emulsions that are stable against coalescence. This synthesis allows for their compression into a biliquid foam structure resembling cohesive tissues, as shown in Fig. 1 B, C.

These emulsions are visualized under a confocal microscope, revealing uniform cadherin fluorescence on the surface of the droplets, as shown in the inset in Fig. 2A. Cadherins depend on calcium ions for their adhesive function (43). Specifically, the ectodomains are comprised of tandem immunoglobulin-like domains that bind calcium, which increases their rigidity to form a crescent shape (44). This conformation enables them to bind other cadherins through *trans* interactions across cells and *cis* interactions on the same cell. Histograms of fluorescence intensity on the droplet surface reveal that adding calcium $[Ca^{2+}]$ increases cadherin surface adsorption. Converting the intensity to protein density ρ (see Methods) allows us to quantify the surface adsorption of bulk cadherin [cad], as shown in Fig. 2B. Both WT and MT data are well fit with the Langmuir adsorption isotherm

$$\frac{\rho}{\rho_{\max}} = \frac{[\mathrm{cad}]K_{eq}}{1 + [\mathrm{cad}]K_{eq}}, \qquad \textbf{(1)}$$

where $\rho_{\max}$ is the cadherin saturation density. Cadherin adsorption via the histidine tag has an equilibrium constant of $K_{eq} = 4 \times 10^{-12}$. Note that in the presence of calcium, cadherin preferentially partitions into the aqueous phase above $[\mathrm{cad}] = 1$ μM, likely due to protein aggregation. We find that adding physiological 1.8mM for $[\mathrm{Ca^{2+}}]$ increases $\rho_{\max}$ by 25%, which corresponds to a decrease in inter-cadherin distance from 9.1 to 8.1, almost reaching the crystalline packing limit at 7.2 (10). The ratio of K_{eq} with and without calcium yields a free energy difference of 0.3 $\mathrm{k_BT}$. This adsorption enhancement may be a consequence of the entropy loss upon calcium stiffening of the proteins, as illustrated in Fig. 2C. The protein concentration does not affect the surface tension because the proteins are not adsorbed at the interface, but are carried by the functionalized lipids (45).

Having characterized the density of proteins on the surface, we demonstrate their adhesive function via an aggregation assay (46). Thermal emulsion droplets of diameter 5 μm, functionalized with either WT or MT, do not adhere in the absence of calcium, nor do they adhere in the presence of calcium without cadherins, as shown in Fig. S3. However, they do bind to form diffusion-limited aggregates (DLA) (47) in the presence of proteins and calcium, as shown in Fig. 2D. These branched structures have on average three droplet neighbors in WT or MT adhesion, consistent with DLA theory, as shown in Fig. 2E.

Using large cadherin-coated droplets the size of biological cells, we study the effects of concentration and applied pressure on cadherin-cadherin adhesion strength in both WT and MT proteins. Gravity alone is insufficient to deform the droplets away from spherical because the kinetic barrier to adhesion is too high. Compression by centrifugation overcomes this barrier by bringing the molecules closer together at a flat interface, activating their adhesion. In fact, applying a centrifugation rate of 800g, corresponding to a compression of 4.8 kPa, deforms the droplets into a foam and facilitates cadherin recruitment into adhesions. We subsequently allow the system to relax for 48h to reach mechanical equilibrium

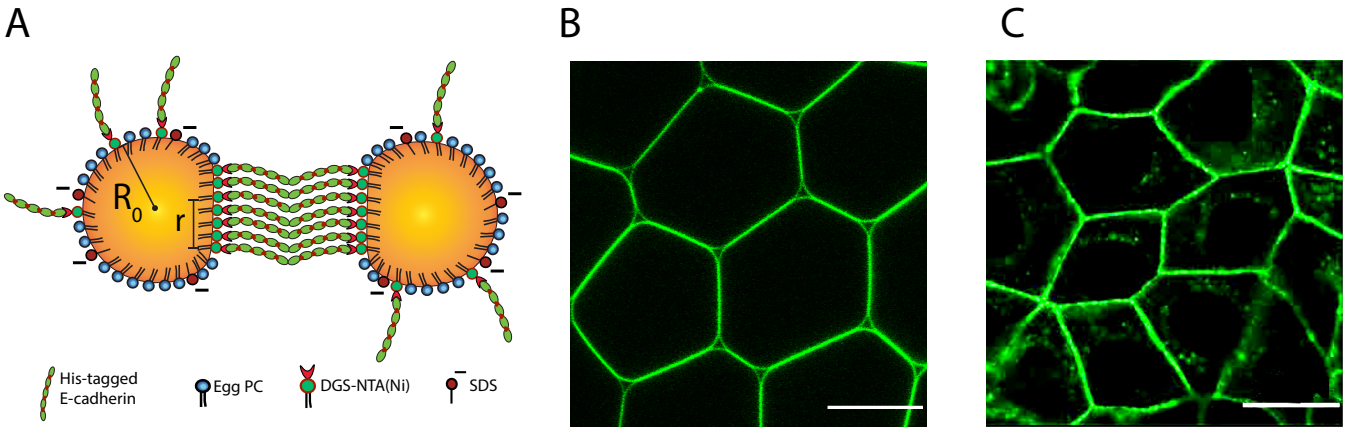

Fig. 1. (A) Schematic representation of biomimetic emulsion droplets. Droplets consist of silicon stabilized through phospholipids and SDS. Lipids with a NTA(Ni) group allow for the binding of His-tagged cadherin ectodomains. (B) Biomimetic emulsion droplets functionalized with fluorescent E-cadherin extracellular domain form a confluent tissue-like structure. (C) Cadherin-expressing living cells form a confluent packing through cadherin binding (40). Scale bar: $20\mu\mathrm{m}$.

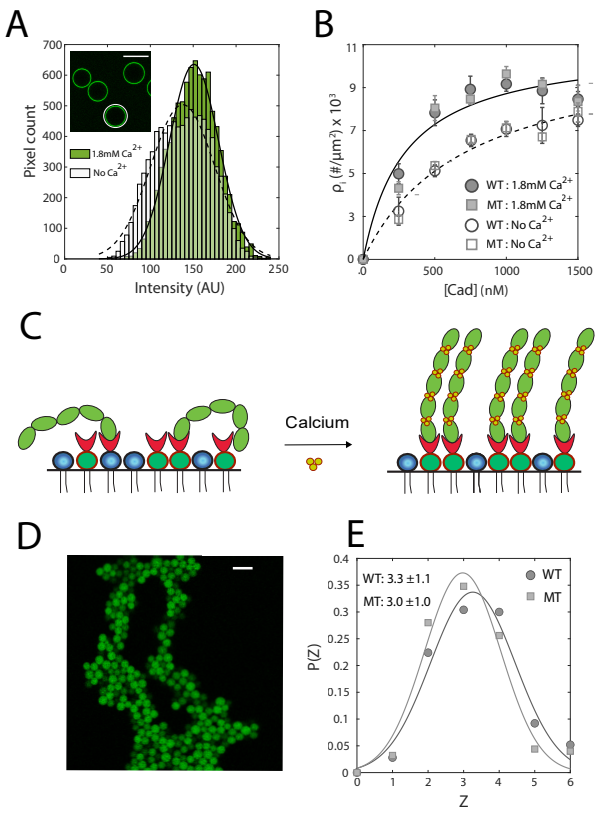

Fig. 2. (A) Distribution of pixel brightness for a given droplet, measured on the focal plane that displays the larger ring diameter. The average intensity in presence of calcium (green histogram) is larger that the average intensity without (white histogram), indicating that calcium favors the recruitment of cadherins at the droplet surface. (B) Cadherin surface adsorption density ρ_i as a function of cadherin bulk concentration [Cad]. Adsorption at the droplet surface increases when bulk density increases, and saturates when [Cad]$\simeq 10^3\mathrm{nM}$. Addition of calcium in the medium yields a higher cadherin surface density up to $\rho_i \simeq 9.3\times10^3\,\mathrm{cad}/^2$. (C) Schematic representation of calcium binding to cadherins. Calcium binding rigidifies cadherins, giving them a crescent shape, which is crucial to forming *trans* dimers. Rigidified cadherins also leave more surface area open for the binding of additional cadherins to the droplet. (D) Cadherin-coated Brownian droplets (green disks) form large aggregates upon calcium addition, confirming homophilic adhesion. Scale bar: 20.(E) Distribution of coordination number for WT and MT cadherin-coated droplets. Both WT and MT form droplet aggregates of mean coordination number $\langle Z\rangle = 3$.

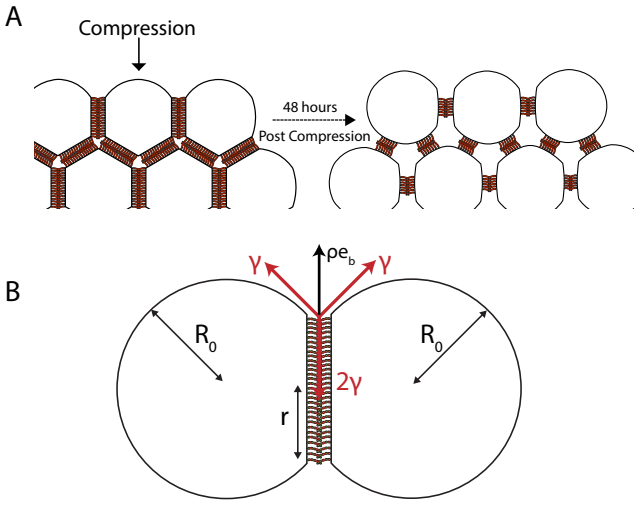

Fig. 3. (A) Droplets adopt a foam-like structure through centrifugation. Over 48 hours, the system relaxes to a foam under tension, where cohesion is maintained by the cadherin-populated patches between neighbouring droplets. Compressed droplets attempt to relax back to spheres under the influence of droplet surface tension and the re-entry of aqueous buffer. (B) Expanded view of the force balance between two adhesive droplets of uncompressed radii R_0 and adhesion radius r, with cadherin density ρ. Mechanical equilibrium is maintained in adhesive droplets through the balance between cadherin binding energy e_b and droplet surface tension γ.

where the surface tension force is balanced by the cadherin binding forces, as shown in Figs. 3A, B. Droplets relax back to spheres in the absence of calcium within 15 minutes, Fig. S4.

Control experiments show that cadherin adhesion is only activated in the presence of calcium, otherwise the droplets return to their spherical shape. With calcium, increasing the initial concentration of cadherins on the surface, ρ_i, stabilizes progressively larger adhesions in both the WT and MT proteins, as shown in Fig. 4A. For each concentration, the adhesive emulsions are refractive index matched for visualization in 3-D (48), as shown in Fig. 4B, C. Image analysis identifies the average intensity and the adhesion area A, which in turn give the density and a corresponding number of cadherins N

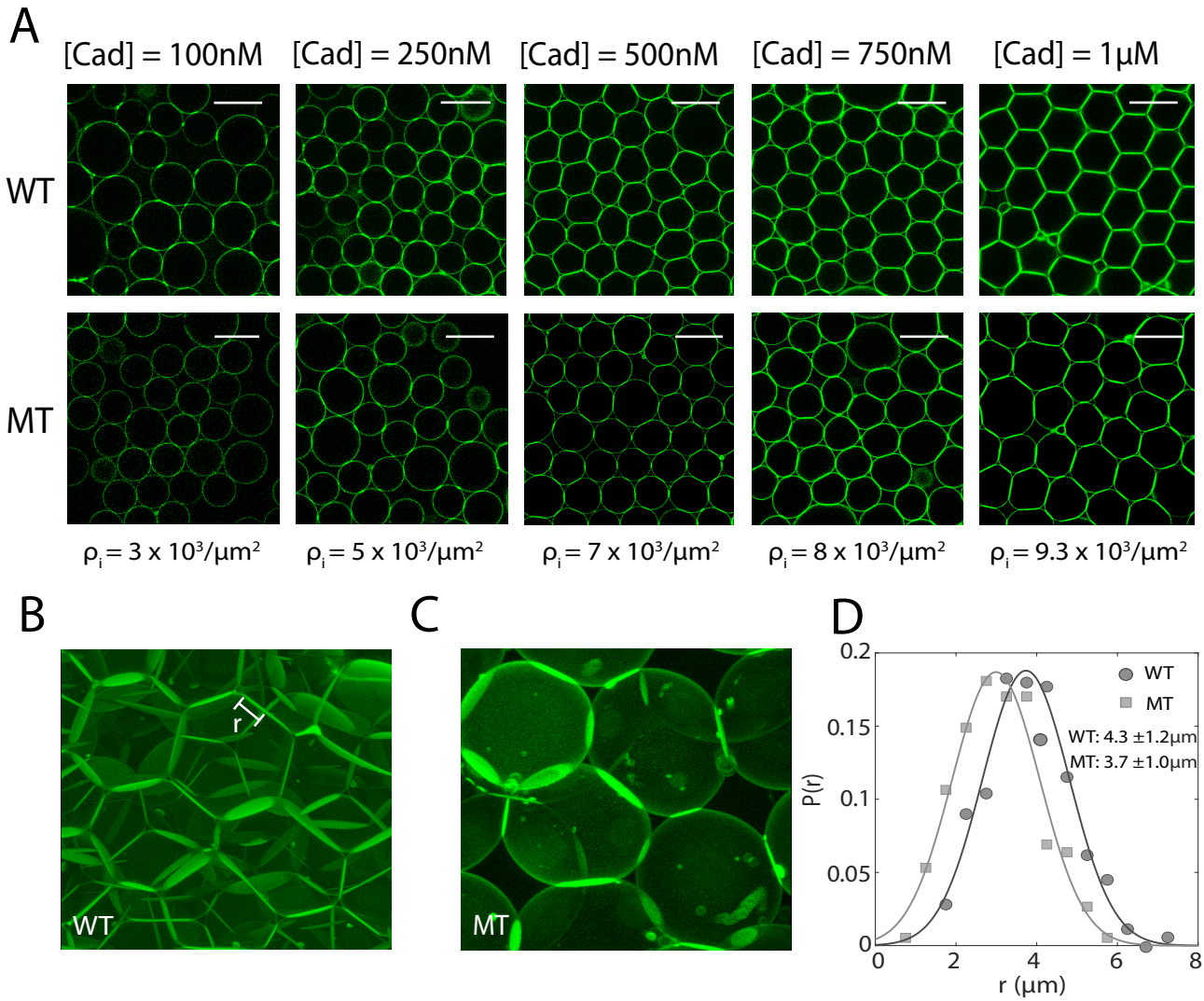

Fig. 4. (A) Final configuration of the system after compression at $4.8\mathrm{kPa}$ and 48h relaxation, for different concentrations of bulk cadherins, both for WT (upper panels) and MT (lower panels). Droplets of varying cadherin surface densities were centrifuged, resulting in the formation of irreversible adhesions and deformations. Scale bar: 20. (B, C) 3-D reconstruction of compressed droplets for WT (panel B) and MT (panel C). Cadherins are concentrated at sites of adhesion upon compression. For each patch, the radius r is measured, and yields the patch area A. Panel width corresponds to $40\mu\mathrm{m}$. (D) Distribution of patch radii for both WT and MT systems. For (B), (C) and (D): surface density $\rho_i = 9.3 \times 10^3 \mathrm{cad}/^2$ and compression $P = 4.8$kPa.

in each adhesion patch. Here N is measured directly from the cadherin fluorescence intensity, and converted to density after mechanical equilibrium is reached. The broad distribution of patch radii arises from the heterogeneous droplet packing geometry and stresses therein (48). Figure 4D shows that the WT on average stabilizes larger patches than the MT under the same experimental conditions.

From these data, we estimate the free energy of binding per molecule e_b. First, we estimate the total deformation energy E_d stored in a system consisting of two droplets in contact. In the limit of small deformations and given a constant surface tension $\gamma = 7 \pm 0.5$ mN/m across the droplet interface (49), we have

$$E_d = \frac{2\gamma}{\mathcal{S}_0} A^2, \qquad \textbf{(2)}$$

where $\mathcal{S}_0 = 4\pi R_0^2$ denotes the area of the spherical droplet of radius R_0 and A is the contact area of adhesion. In mechanical equilibrium, this energy of deformation is balanced by the total free energy of binding $N \times e_b$ of N cadherin molecules. Using Eq. (2), the binding energy per cadherin bond e_b is thus given by

$$e_b = \frac{2\gamma A^2}{\mathcal{S}_0 N}. \qquad \textbf{(3)}$$

This result predicts $A = \left(\frac{e_b \mathcal{S}_0}{2\gamma}\right)^{1/2} N^{1/2}$ or equivalently $A = \frac{e_b \mathcal{S}_0}{2\gamma}\rho$, where ρ is the cadherin density in the patch. In Fig. 5A, this linear increase of area with density holds in the limit of low initial concentrations ρ_i (under 4.8 kPa compression) and gives $e_b = 1.6 \pm 0.3$ $\mathrm{k_B T}$ in the case of the MT. This free energy of *trans* binding alone is in the range predicted by computational studies that take into account the rotational and vibrational entropy loss upon confinement and dimerization in 2D (50).

Above a threshold ρ, the cadherins jam into patches of a con-

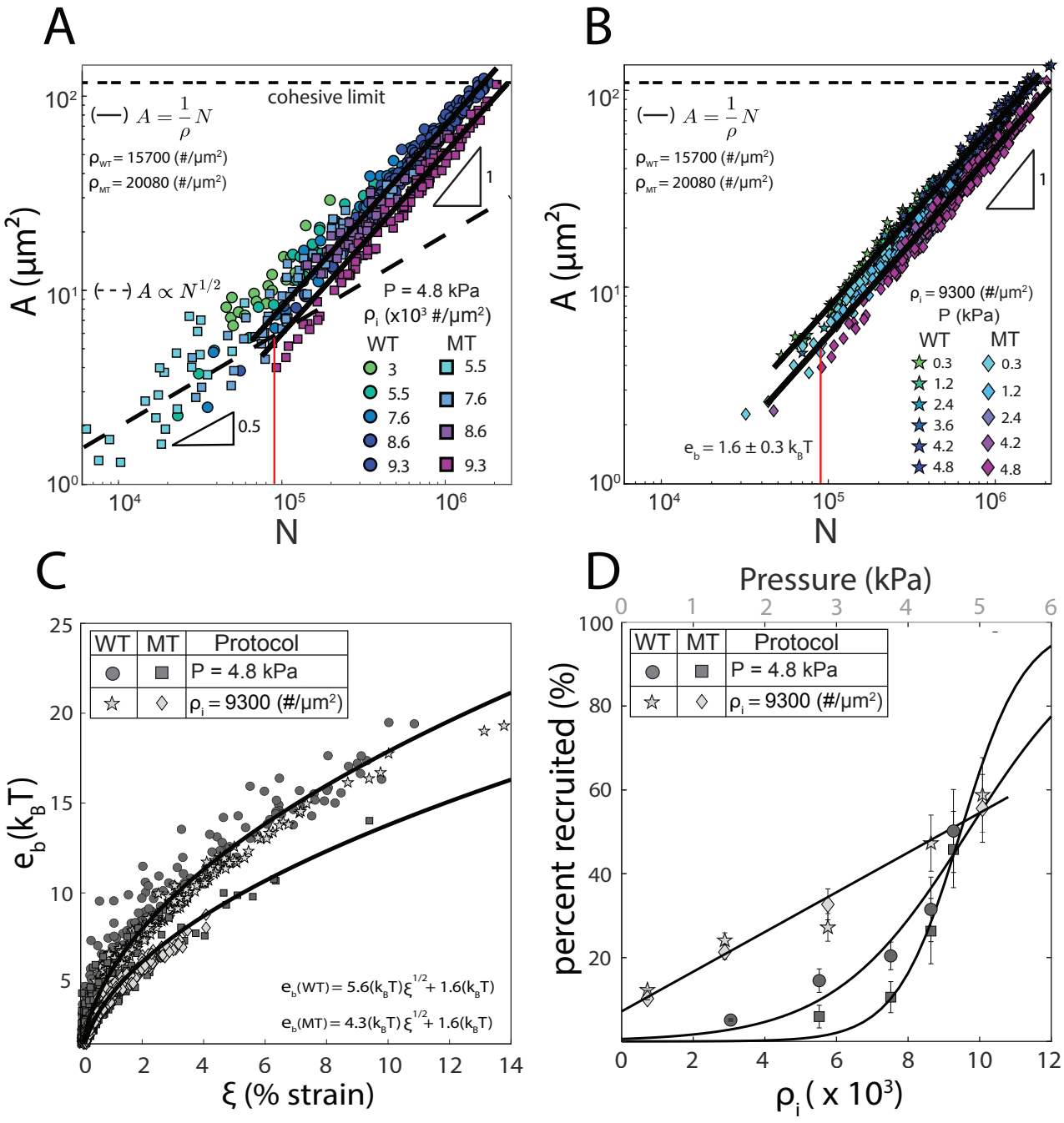

Fig. 5. (A) Area A of patches as a function of cadherin number N in the patch for different cadherin surface concentration ρ_i in WT and MT systems, at a given compression $P = 4.8$kPa. We identify two regimes. For low cadherin number, the data follows $A \propto N^{1/2}$ (black dashed line), yielding an estimate of $e_b = 1.6 \pm 0.3\ k_BT$. For larger N, the data follows $A \propto N$, indicating constant density in the patches. (B) Area of patches A, as a function of the number of cadherins N in the patch for fixed cadherin surface concentration ρ_i and different values of compression. The compression ranges from about 0.3 to 4.8 kPa. For both WT and MT, we observe $A \propto N$, indicating that adhesions are growing at a constant density. For the WT the density is $\rho_{\rm WT} = 15.7 \times 10^3 {\rm cad}/\mu{\rm m}^2$, while the MT adhesions are denser at about $\rho_{\rm MT} = 20.1 \times 10^3 {\rm cad}/\mu{\rm m}^2$. (C) Binding energy e_b per cadherin bond as a function of the area strain ξ of the deformed droplets, for both pressure and density evolution as shown in in panel A and B. Since $e_b = 2\gamma A^2/(N\mathcal{S}_0)$ and $A = \rho N$ with constant density, e_b varies with deformation (D) Fraction of cadherins recruited as a function of varying cadherin density and pressure. Circles (WT) and squares (MT) show cadherin recruitment as a function of cadherin density (ρ_i). An empirical fit demonstrates the sigmoidal nature of the recruitment with an inflection point around $9500{\rm cad}/^2$. Stars (WT) and diamonds (MT) show recruitment evolution as a function of applied pressure (top axis). Varying the pressure from 0.3 to 4.8 kPa leads to a linear growth in recruitment for both WT and MT.

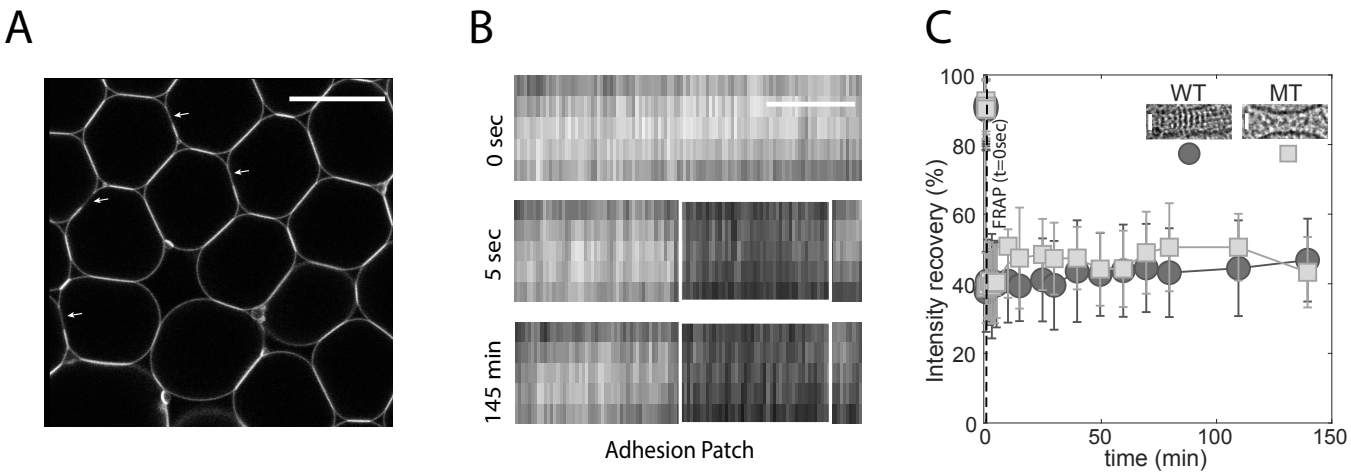

Fig. 6. (A) Focus on a loosely packed region in the capillary for WT cadherin-saturated droplets ($\rho_i = 9.3 \times 10^3 \mathrm{cad}/\mu\mathrm{m}^2$) and maximal compression at $P = 4.8\mathrm{kPa}$. Arrows indicate photobleached regions on adhesion patches. Scale bar: $20\mu\mathrm{m}$. (B) Magnified view of an adhesion before and after FRAP. Scale bar: $1\mu\mathrm{m}$. The photobleached regions of patches do not recover initial intensity, for both WT and MT, indicating a jammed state in the patches in both situations. (C) Quantitative measurement of recovery intensity after FRAP, for both WT and MT. Inset: electron-microscopy of patches made of WT or MT, reproduced from (10).

stant density ($A \propto N$) $\rho_{\mathrm{MT}} = 20.1 \times 10^3/\mu\mathrm{m}^2$. Increasing ρ_i enhances the probability to make larger adhesion patches, but does not change their density. This MT density corresponds to an average inter-cadherin distance of $6.9 \pm 0.1\mathrm{nm}$, which agrees with the jamming limit of the random packing of disks (51). On the other hand, WT adhesions are comprised of both *cis* and *trans*-interacting cadherins, which forces them to crystallize at a lower density of $\rho_{\mathrm{WT}} = 15.7 \times 10^3/\mu\mathrm{m}^2$, also shown in the figure. This patch density is independent of initial concentration. It corresponds to an inter-cadherin distance of $7.9\ \mathrm{nm}$, which is in good agreement with the reported crystal lattice distances of 7.2 to $7.9\ \mathrm{nm}$, as measured by crystallography or electron microscopy of liposome and cell-cell adhesions (10, 52).

Assuming a constant e_b per molecule in Eq. (3), a given cadherin density fixes the area of deformation. However, our data shows that patches of the same density give rise to increasing adhesion sizes as a function of the applied pressure. We therefore interpret our experimental results in terms of the e_b increase with droplet deformation, quantified as the area strain of a droplet,

$$\xi = \frac{\mathcal{S} - \mathcal{S}_0}{\mathcal{S}_0}, \qquad \textbf{(4)}$$

where $\mathcal{S}$ denotes the area of the deformed droplet and, in the limit of small deformations, $\mathcal{S} - \mathcal{S}_0 = \sum_{i=1}^{n} A_i^2/\mathcal{S}_0$ (53), where index i labels the patches on a droplet with n contacts. In the limit of maximum compression into a biliquid foam, we measure the number of contacts per droplet $n = 12$ (54, 55), and we can thus set the local strain of a contact patch of area A to be $\xi \simeq 12A^2/\mathcal{S}_0^2$.

To maximize the extent of adhesion we saturate ρ_i to $9.3 \times 10^3/\mu\mathrm{m}^2$, and test the effect of the applied pressure ranging from 0.3 kPa to 4.8 kPa. In Fig. 5B, we show the same linear increase of A vs. N, i.e., constant cadherin packing density, for the WT and MT as those observed in Fig. 5A, confirming protein crystallization or jamming, respectively. Increasing the pressure forms progressively larger adhesion areas, similar to the effect of increasing ρ_i at constant pressure in Fig. 5A. Both ρ_i and the applied pressure, therefore, play an important role in stabilizing adhesions.

We find $e_b \propto \xi^{1/2}$, see Fig. 5C. This result is indicative of a force-dependent adhesion response, where the cadherin-dimer bond is strengthened in response to deformation (29). While both WT and MT show a continuously increasing binding free energy, the WT stabilizes larger adhesion patches than the MT and reaches higher binding energies of up to $20\mathrm{k_B T}$ at the cohesive droplet limit. The amplitude of the stress response of the MT is $3/4$ of that of the WT, highlighting the importance of *cis* and *trans* cooperativity in stabilizing adhesion.

To test the validity of the measured strengthening of Cadherin bonds, we perform a negative control using binders that have no known mechano-sensitive property. This experiment is realized using complementary single DNA strands on neighboring droplets, shown in the schematic in Fig. S5. When they are in contact, the DNA hybridizes causing adhesion between droplets. The DNA binding is not mechano-sensitive: adhesions are formed spontaneously without the need for compression. In addition, compression and subsequent relaxation do not significantly change the adhesion size/strength. Analyzing the growth of the area of adhesion as a function of the number of molecules N in the patch reveals the $A \propto N^{1/2}$ relation (see Figures S6A,B), indicative of a fixed free energy of binding per molecule, instead of the linear relation found in cadherins.

Next, we plot the percentage of recruited proteins into adhesions as a function of both pressure and concentration, see Fig. 5D. Since increasing pressure linearly increases the area of adhesion, it also linearly increases the fraction of recruited molecules, consistent with a random attachment model at fixed concentration. Conversely, increasing ρ_i at fixed pressure, we observe a sharp non-linear increase in recruitment for both WT and MT above a common threshold density, see Fig. 5D. This behavior is reminiscent of a density-dependent phase-transition that has been predicted to occur in cadherin

ectodomains (13, 39).

Our density measurements in Fig. 5 suggest that WT and MT adhesions are solid-like, either in a crystalline or a randomly jammed array. To test this hypothesis, we FRAP sections of many adhesion zones, as shown in Fig. 6A. Both protein types do not fully bleach, but preserve 40% of the initial fluorescence after a one minute laser pulse Fig. 6B,C. We do not observe any subsequent fluorescence recovery, consistent with solid adhesions. However, bleaching the proteins that are outside the adhesions uncovers two cadherin populations that recover over significantly different timescales, $\tau_1 = 44$ s and $\tau_2 = 523$ s, respectively. Their diffusion constants, given by $D = r_b^2/(4\tau)$, where r_b is the radius of the circular photobleached region, yield $D_1 = 2.2 \times 10^{-2}$ μm^2/s and $D_2 = 2.0 \times 10^{-3}$ μm^2/s, Fig. S7. The fast recovery is consistent with the diffusion of lipids on the surface of a silicon oil emulsion (56), while the slow recovery may be a result of lateral crowding interactions at the saturation cadherin ρ_i used in these experiments.

Discussion

In this paper, we have established that our biomimetic emulsion system can recapitulate a number of known E-cadherin-dependent phenomena and thus constitutes a useful platform to study cadherin-mediated cell-cell adhesion. First, we quantify the effect of calcium on the packing density of cadherins at droplet interfaces and establish its role in enabling *trans* dimerization. Second, as observed in cells, WT cadherins coated on droplet surfaces spontaneously organize into adhesions with a crystalline density, driven by both *trans* and *cis* interactions. Third, we find that the MT does not form a crystalline lattice, but, rather, jams into clusters with a higher density than the WT. This tendency of the MT to form dense adhesions through non-specific lateral interactions has also been observed previously in lipid bilayer systems (57).

Both WT cadherins and the *cis* mutant are found to be mechanosensitive, but the WT cadherins are able to reach a higher binding energy of $20 k_B T$ compared to $14 k_B T$ for the MT. This enhancement may be due to *cis* and *trans*-cooperativity in the WT, in agreement with FRET-based measurements showing that bond-lifetimes are greatly increased due to *cis* interactions (32). While it is known that cadherins are capable of force-dependent tuning of their adhesion by acting like catch-bonds under tensile stress(27–29, 58, 59), rigorously defined as an increase in lifetime with increasing force (60), further experiments are necessary to pinpoint the molecular mechanism associated with this phenomenon. A plausible candidate has been identified as the X-dimer configuration of bound E-cadherin (61, 62). Our system opens the door to further experiments with mutant proteins aimed at directly establishing a role for X-dimers in the E-cadherin mechanosensitive response and, more generally, in regulating the transmission of forces between cells.

Materials and Methods

Emulsion Preparation. The protocol for the emulsion preparation is described in (30). Briefly, the oil droplets are co-stabilized with SDS (1 mM) and the following mixtures of lipids: EPC (egg phosphatidylcholine) and DGS-NTA (Ni) lipids at a molar ratio of 92:8. The lipids were purchased from Avanti Polar Lipids (St. Louis, MO). They were mixed to reach a total mass of about 14 mg and dried under nitrogen before the addition of 10 mL 50-cSt silicone oil purchased from Sigma Aldrich (St. Louis, MO). The lipid-containing oil was then sonicated for 30 min at room temperature and heated for 3 hours at $50°$C. We thus obtained an oil saturated with phospholipids. The lipid-containing oil (10 mL) was then emulsified through a microfluidic chip. The resulting emulsion was mono-disperse with a diameter of about 20 μm. Brownian emulsion droplets were produced through membrane emulsification by a 0.5 μm pore membrane (SPG Technology, Miyazaki, Japan), with 10 mM SDS as the continuous phase, which resulted in droplets with a diameter of approximate $4 - 5$ μm. To functionalize these droplets with DGS-NTA(Ni), 0.5 mg of DGS-NTA(Ni) was dried and rehydrated with binding buffer and droplets at a $1:1$ ratio. The droplets were incubated with the phospholipid and binding buffer mix overnight at room temperature and gentle rotation.

Cadherin Grafting. Binding buffer was prepared containing 3.8mM calcium, 2 mM EDTA, 20 mM Tris, 10 mM NaCl, 10 mM KCl, pH = 7, and 1 mM SDS in a 50:50 glycerol/water solution for refractive index matching. The emulsion was mixed with binding buffer at 40% volume fraction and then incubated with varying concentrations of His-tagged E-cadherin ectodomains in 50 μL of binding buffer containing EDTA. Low concentrations of salts were added to reduce nonspecific adhesions between the droplets.

Cadherin Density Estimation. We experimentally measured the density of cadherins on the droplet surface at droplet saturation. The fluorescence intensity of a solution of 1 μM WT E-cadherin, containing 3.0×10^{13} molecules was measured through a fluorimeter (Horiba-PTI QM-400 Fluorescent spectrometer). Upon adding droplets at 40% volume fraction and 1.8 mM calcium, we observed a 62% loss in fluorescence intensity of the 1 μM cadherin solution. This loss of intensity from the bulk solution indicated that approximately 1.8×10^{13} cadherin molecules migrated from the bulk solution on to the droplets. We estimated the droplet density to be about 3.2×10^4 $/\mu$l, corresponding to a total droplet count of about 1.6×10^6 in a 50μl sample. Therefore, there were approximately 1.2×10^7 cadherin molecules per droplet. For a droplet of radius 10 μm, the surface area is 1256 μm^2. The density of cadherins at saturation is approximately 9.3×10^3 $/\mu$m^2. Therefore, a saturation intensity of 150 A.U. for WT cadherin and 120 A.U. for MT cadherin corresponded to a cadherin surface density of 9.3×10^4 $/\mu$m^2. The fluorescence measurements are shown in Fig. S1.

Confocal Microscopy. The droplets were grafted with cadherin proteins which were fluorescently labeled with Alexa 488. The buffer was refractive index matched with glycerol for transparency, which allowed for imaging of the emulsion in 3-D. We used a fast-scanning confocal microscope (TCS SP5 II; Leica Microsystems, Buffalo Grove, IL)

Centrifugation and Pressure Measurement. The experimental setup involved cadherin-functionalized droplets contained in a capillary, $5\mathrm{mm}$ and $100\mu\mathrm{m}$ in depth (VitroTubes, NJ). The droplets in the capillary were compressed in a centrifuge at speeds ranging from $50g$ up to $800g$, after which they were allowed to relax over a 48-hour period. The pressure inside the compressed aggregate was estimated through the relation $P = \Delta\rho g h$, where P is the hydrostatic pressure, $\Delta\rho$ is the density difference between silicon oil and water, and h is the height of the compressed aggregate pile which was measured after centrifugation and equilibration of droplets.

Fluorescence Recovery after Photobleaching (FRAP). Droplets functionalized with cadherin were placed in a glass capillary. The droplet-containing capillaries were centrifuged at $800\mathrm{g}$ to form a cohesive 3-D droplet aggregate, which was then visualized through confocal microscopy. Suitable adhesions and free perimeters were identified and marked as regions of interest. A laser pulse of $\sim 200\mathrm{mW}$ was applied for 1.5 minutes to the FRAP region of interest in order to photobleach. FRAP intensity trajectories were fit using custom MATLAB code that subtracted background, normalized the intensities to their pre-bleach level, and fit to an exponential model $I = I_{\max}(1 - e^{-t/\tau})$, where I is the normalized intensity, $I_{\max}$ is the pre-photobleach intensity, t is time, and τ is the characteristic recovery time.

Author Contributions

L.S., B.H., L-.L.P., and J.B. designed the study and wrote the paper. K.N. designed the study, performed experiments, analyzed experimental data and wrote the paper. A.I. analyzed experimental data. R.Z. developed theory. L.F. analyzed experimental data. O.J.H. expressed and purified proteins.

Acknowledgments

We thank Sergey Troyanovsky, Angus McMullen, and Sascha Hilgenfeldt for helpful discussions. This work was supported by the NIH Molecular Biophysics Training Grant T32 GM088118 to K.N., NSF MCB 19101542, the Paris Region (Région Île-de-France) under the Blaise Pascal International Chairs of Excellence to J.B. and N.B.J, the Emergence(s) grant from the Ville de Paris to L-L P, NIH R01MH114817 to L.S. and O.J.H, and the National Science Foundation under grants No. NSF PHY17-48958 and No. NSF DMR-1710163 to BH.

Competing Interests

The authors declare no competing interests

Bibliography

1. M Takeichi. The cadherins: cell-cell adhesion molecules controlling animal morphogenesis. *Development*, 102(4):639–655, April 1988.
2. Jennifer M. Halbleib and W. James Nelson. Cadherins in development: cell adhesion, sorting, and tissue morphogenesis. *Genes & Development*, 20(23):3199–3214, December 2006. ISSN 0890-9369, 1549-5477. doi: 10.1101/gad.1486806.
3. Carien M. Niessen, Deborah Leckband, and Alpha S. Yap. Tissue Organization by Cadherin Adhesion Molecules: Dynamic Molecular and Cellular Mechanisms of Morphogenetic Regulation. *Physiological Reviews*, 91(2):691–731, April 2011. ISSN 0031-9333. doi: 10.1152/physrev.00004.2010.
4. Floor Twiss and Johan de Rooij. Cadherin mechanotransduction in tissue remodeling. *Cellular and Molecular Life Sciences*, 70(21):4101–4116, November 2013. ISSN 1420-9071. doi: 10.1007/s00018-013-1329-x.
5. Jean-Léon Maître and Carl-Philipp Heisenberg. Three Functions of Cadherins in Cell Adhesion. *Current Biology*, 23(14):R626–R633, July 2013. ISSN 0960-9822. doi: 10.1016/j.cub.2013.06.019.
6. Marita Goodwin and Alpha S. Yap. Classical cadherin adhesion molecules: coordinating cell adhesion, signaling and the cytoskeleton. *Journal of Molecular Histology*, 35(8-9):839–844, November 2004. ISSN 1567-2379, 1573-6865. doi: 10.1007/s10735-004-1833-2.
7. K. Venkatesan Iyer, Romina Piscitello-Gómez, Joris Paijmans, Frank Jülicher, and Suzanne Eaton. Epithelial Viscoelasticity Is Regulated by Mechanosensitive E-cadherin Turnover. *Current Biology*, 29(4):578–591.e5, February 2019. ISSN 0960-9822. doi: 10.1016/j.cub.2019.01.021.
8. Yuliya I. Petrova, Leslayann Schecterson, and Barry M. Gumbiner. Roles for E-cadherin cell surface regulation in cancer. *Molecular Biology of the Cell*, 27(21):3233–3244, November 2016. ISSN 1059-1524. doi: 10.1091/mbc.E16-01-0058.
9. Michalina Janiszewska, Marina Candido Primi, and Tina Izard. Cell adhesion in cancer: Beyond the migration of single cells. *The Journal of biological chemistry*, 295:2495–2505, 2 2020. ISSN 1083-351X. doi: 10.1074/JBC.REV119.007759.
10. Oliver J. Harrison, Xiangshu Jin, Soonjin Hong, Fabiana Bahna, Goran Ahlsen, Julia Brasch, Yinghao Wu, Jeremie Vendome, Klara Felsovalyi, Cheri M. Hampton, Regina B. Troyanovsky, Avinoam Ben-Shaul, Joachim Frank, Sergey M. Troyanovsky, Lawrence Shapiro, and Barry Honig. The Extracellular Architecture of Adherens Junctions Revealed by Crystal Structures of Type I Cadherins. *Structure*, 19(2):244–256, February 2011. ISSN 0969-2126. doi: 10.1016/j.str.2010.11.016.
11. Barry Honig and Lawrence Shapiro. Adhesion protein structure, molecular affinities, and principles of cell-cell recognition. *Cell*, 181(3):520–535, April 2020.
12. P. Katsamba, K. Carroll, G. Ahlsen, F. Bahna, J. Vendome, S. Posy, M. Rajebhosale, S. Price, T. M. Jessell, A. Ben-Shaul, L. Shapiro, and Barry H. Honig. Linking molecular affinity and cellular specificity in cadherin-mediated adhesion. *Proceedings of the National Academy of Sciences*, 106(28):11594–11599, July 2009. ISSN 0027-8424, 1091-6490. doi: 10.1073/pnas.0905349106.
13. Yinghao Wu, Xiangshu Jin, Oliver Harrison, Lawrence Shapiro, Barry H. Honig, and Avinoam Ben-Shaul. Cooperativity between trans and cis interactions in cadherin-mediated junction formation. *Proceedings of the National Academy of Sciences*, 107(41):17592–17597, October 2010. ISSN 0027-8424, 1091-6490. doi: 10.1073/pnas.1011247107.
14. A S Yap, C M Niessen, and B M Gumbiner. The juxtamembrane region of the cadherin cytoplasmic tail supports lateral clustering, adhesive strengthening, and interaction with p120ctn. *J. Cell Biol.*, 141(3):779–789, May 1998.
15. Binh-An Truong Quang, Madhav Mani, Olga Markova, Thomas Lecuit, and Pierre-François Lenne. Principles of E-Cadherin Supramolecular Organization In Vivo. *Current Biology*, 23 (22):2197–2207, November 2013. ISSN 0960-9822. doi: 10.1016/j.cub.2013.09.015.
16. Hong, S, Regina B. Troyanovsky, and Sergey M. Troyanovsky. Binding to F-actin guides cadherin cluster assembly, stability, and movement. *Journal of Cell Biology*, 201(1):131–143, April 2013. doi: 10.1083/jcb.201211054.
17. Zhijun Liu, John L Tan, Daniel M Cohen, Michael T Yang, Nathan J Sniadecki, Sami Alom Ruiz, Celeste M Nelson, and Christopher S Chen. Mechanical tugging force regulates the size of cell-cell junctions. *Proc. Natl. Acad. Sci. U. S. A.*, 107(22):9944–9949, June 2010.
18. Benoit Ladoux, Ester Anon, Mireille Lambert, Aleksandr Rabodzey, Pascal Hersen, Axel Buguin, Pascal Silberzan, and René-Marc Mège. Strength dependence of cadherin-mediated adhesions. *Biophys. J.*, 98(4):534–542, February 2010.
19. Hamid Tabdili, Matthew Langer, Quanming Shi, Yeh-Chuin Poh, Ning Wang, and Deborah Leckband. Cadherin-dependent mechanotransduction depends on ligand identity but not affinity. *J. Cell Sci.*, 125(Pt 18):4362–4371, September 2012.
20. William A Thomas, Cécile Boscher, Yeh-Shiu Chu, Damien Cuvelier, Clara Martinez-Rico, Rima Seddiki, Julie Heysch, Benoit Ladoux, Jean Paul Thiery, René-Marc Mege, and Sylvie Dufour. α-Catenin and vinculin cooperate to promote high e-cadherin-based adhesion strength. *J. Biol. Chem.*, 288(7):4957–4969, February 2013.
21. Quint le Duc, Quanming Shi, Iris Blonk, Arnoud Sonnenberg, Ning Wang, Deborah Leckband, and Johan de Rooij. Vinculin potentiates e-cadherin mechanosensing and is recruited to actin-anchored sites within adherens junctions in a myosin II-dependent manner. *J. Cell Biol.*, 189(7):1107–1115, June 2010.
22. Adrienne K Barry, Hamid Tabdili, Ismaeel Muhamed, Jun Wu, Nitesh Shashikanth, Guillermo A Gomez, Alpha S Yap, Cara J Gottardi, Johan de Rooij, Ning Wang, and Deborah E Leckband. A-catenin cytomechanics–role in cadherin-dependent adhesion and mechanotransduction. *J. Cell Sci.*, 127(Pt 8):1779–1791, April 2014.
23. Caitlin Collins, Aleksandra K. Denisin, Beth L. Pruitt, and W. James Nelson. Changes in E-cadherin rigidity sensing regulate cell adhesion. *Proceedings of the National Academy of Sciences of the United States of America*, 114(29):E5835–E5844, July 2017. ISSN 0027-8424. doi: 10.1073/pnas.1618676114.
24. Shigenobu Yonemura, Yuko Wada, Toshiyuki Watanabe, Akira Nagafuchi, and Mai Shibata. α-catenin as a tension transducer that induces adherens junction development. *Nature Cell Biology 2010 12:6*, 12:533–542, 5 2010. ISSN 1476-4679. doi: 10.1038/ncb2055.
25. Nicolas Borghi, Maria Sorokina, Olga G Shcherbakova, William I Weis, Beth L Pruitt, W James Nelson, and Alexander R Dunn. E-cadherin is under constitutive actomyosin-

generated tension that is increased at cell-cell contacts upon externally applied stretch. *Proc. Natl. Acad. Sci. U. S. A.*, 109(31):12568–12573, July 2012.
26. Rima Seddiki, Gautham Hari Narayana Sankara Narayana, Pierre Olivier Strale, Hayri Emrah Balcioglu, Grégoire Peyret, Mingxi Yao, Anh Phuong Le, Chwee Teck Lim, Jie Yan, Benoit Ladoux, and René Marc Mège. Force-dependent binding of vinculin to α-catenin regulates cell–cell contact stability and collective cell behavior. *Molecular Biology of the Cell*, 29:380, 2 2018. ISSN 19394586. doi: 10.1091/MBC.E17-04-0231.
27. Kristine Manibog, Hui Li, Sabyasachi Rakshit, and Sanjeevi Sivasankar. Resolving the molecular mechanism of cadherin catch bond formation. *Nature Communications*, 5(1), September 2014. ISSN 2041-1723. doi: 10.1038/ncomms4941.
28. Kristine Manibog, Kannan Sankar, Sun-Ae Kim, Yunxiang Zhang, Robert L. Jernigan, and Sanjeevi Sivasankar. Molecular determinants of cadherin ideal bond formation: Conformation-dependent unbinding on a multidimensional landscape. *Proceedings of the National Academy of Sciences*, 113(39):E5711–E5720, September 2016. ISSN 0027-8424, 1091-6490. doi: 10.1073/pnas.1604012113.
29. Sabyasachi Rakshit, Yunxiang Zhang, Kristine Manibog, Omer Shafraz, and Sanjeevi Sivasankar. Ideal, catch, and slip bonds in cadherin adhesion. *Proceedings of the National Academy of Sciences*, 109(46):18815–18820, November 2012. ISSN 0027-8424, 1091-6490. doi: 10.1073/pnas.1208349109.
30. Lea-Laetitia Pontani, Ivane Jorjadze, and Jasna Brujic. Cis and Trans Cooperativity of E-Cadherin Mediates Adhesion in Biomimetic Lipid Droplets. *Biophysical Journal*, 110(2): 391–399, January 2016. ISSN 0006-3495. doi: 10.1016/j.bpj.2015.11.3514.
31. P.-H. Puech, H. Feracci, and F. Brochard-Wyart. Adhesion between Giant Vesicles and Supported Bilayers Decorated with Chelated E-Cadherin Fragments. *Langmuir*, 20(22): 9763–9768, October 2004. ISSN 0743-7463. doi: 10.1021/la048682h.
32. Connor J. Thompson, Vinh H. Vu, Deborah E. Leckband, and Daniel K. Schwartz. Cadherin cis and trans interactions are mutually cooperative. *Proceedings of the National Academy of Sciences*, 118(10):e2019845118, March 2021. ISSN 0027-8424, 1091-6490. doi: 10.1073/pnas.2019845118.
33. Kabir H. Biswas, Kevin L. Hartman, Cheng-han Yu, Oliver J. Harrison, Hang Song, Adam W. Smith, William Y. C. Huang, Wan-Chen Lin, Zhenhuan Guo, Anup Padmanabhan, Sergey M. Troyanovsky, Michael L. Dustin, Lawrence Shapiro, Barry Honig, Ronen Zaidel-Bar, and Jay T. Groves. E-cadherin junction formation involves an active kinetic nucleation process. *Proceedings of the National Academy of Sciences*, 112(35):10932–10937, September 2015. ISSN 0027-8424, 1091-6490. doi: 10.1073/pnas.1513775112.
34. Yu Cai, Nitesh Shashikanth, Deborah E. Leckband, and Daniel K. Schwartz. Cadherin Diffusion in Supported Lipid Bilayers Exhibits Calcium-Dependent Dynamic Heterogeneity. *Biophysical Journal*, 111(12):2658–2665, December 2016. ISSN 0006-3495. doi: 10.1016/j.bpj.2016.10.037.
35. Susanne F. Fenz, Timo Bihr, Daniel Schmidt, Rudolf Merkel, Udo Seifert, Kheya Sengupta, and Ana-Sunčana Smith. Membrane fluctuations mediate lateral interaction between cadherin bonds. *Nature Physics*, 13(9):906–913, September 2017. ISSN 1745-2473, 1745-2481. doi: 10.1038/nphys4138.
36. B. Ladoux, W. J. Nelson, J. Yan, and R. M. Mège. The mechanotransduction machinery at work at adherens junctions. *Integrative Biology*, 7(10):1109–1119, October 2015. ISSN 1757-9708. doi: 10.1039/c5ib00070j.
37. Suzie Verma, Annette M Shewan, Jeanie A Scott, Falak M Helwani, Nicole R den Elzen, Hiroaki Miki, Tadaomi Takenawa, and Alpha S Yap. Arp2/3 activity is necessary for efficient formation of e-cadherin adhesive contacts. *J. Biol. Chem.*, 279(32):34062–34070, August 2004.
38. Nadia Efimova and Tatyana M. Svitkina. Branched actin networks push against each other at adherens junctions to maintain cell–cell adhesion. *Journal of Cell Biology*, 217(5):1827–1845, March 2018. ISSN 0021-9525. doi: 10.1083/jcb.201708103.
39. Yinghao Wu, Barry Honig, and Avinoam Ben-Shaul. Theory and Simulations of Adhesion Receptor Dimerization on Membrane Surfaces. *Biophysical Journal*, 104(6):1221–1229, March 2013. ISSN 0006-3495. doi: 10.1016/j.bpj.2013.02.009.
40. Rashmi Priya, Xuan Liang, Jessica L. Teo, Kinga Duszyc, Alpha S. Yap, and Guillermo A. Gomez. ROCK1 but not ROCK2 contributes to RhoA signaling and NMIIA-mediated contractility at the epithelial zonula adherens. *Molecular Biology of the Cell*, 28(1):12–20, January 2017. ISSN 1059-1524, 1939-4586. doi: 10.1091/mbc.e16-04-0262.
41. Jelske N. van der Veen, John P. Kennelly, Sereana Wan, Jean E. Vance, Dennis E. Vance, and René L. Jacobs. The critical role of phosphatidylcholine and phosphatidylethanolamine metabolism in health and disease. *Biochimica et Biophysica Acta (BBA) - Biomembranes*, 1859(9, Part B):1558–1572, September 2017. ISSN 0005-2736. doi: 10.1016/j.bbamem.2017.04.006.
42. Gregor Cevc and Derek Marsh. *Phospholipid bilayers*. Membrane Transport in the Life Sciences Series. John Wiley & Sons, Nashville, TN, June 1987.
43. Bhushan Nagar, Michael Overduin, Mitsuhiko Ikura, and James M. Rini. Structural basis of calcium-induced E-cadherin rigidification and dimerization. *Nature*, 380(6572):360–364, March 1996. ISSN 1476-4687. doi: 10.1038/380360a0.
44. Lawrence Shapiro and William I. Weis. Structure and Biochemistry of Cadherins and Catenins. *Cold Spring Harbor Perspectives in Biology*, 1(3):a003053, September 2009. ISSN , 1943-0264. doi: 10.1101/cshperspect.a003053.
45. Otger Campàs, Tadanori Mammoto, Sean Hasso, Ralph A Sperling, Daniel O'Connell, Ashley G Bischof, Richard Maas, David A Weitz, L Mahadevan, and Donald E Ingber. Quantifying cell-generated mechanical forces within living embryonic tissues. *Nat. Methods*, 11(3): 349–349, March 2014.
46. Michelle R. Emond and James D. Jontes. Bead Aggregation Assays for the Characterization of Putative Cell Adhesion Molecules. *Journal of Visualized Experiments : JoVE*, 92, October 2014. ISSN 1940-087X. doi: 10.3791/51762.
47. Clair R. Seager and Thomas G. Mason. Slippery diffusion-limited aggregation. *Physical Review E*, 75(1):011406, January 2007. ISSN 1539-3755, 1550-2376. doi: 10.1103/PhysRevE.75.011406.
48. Jasna Brujić, Sam F. Edwards, Dmitri V. Grinev, Ian Hopkinson, Djordje Brujić, and Hernán A. Makse. 3D bulk measurements of the force distribution in a compressed emulsion system. *Faraday Discussions*, 123(0):207–220, 2003. doi: 10.1039/B204414E. Publisher: Royal Society of Chemistry.
49. L.-L. Pontani, I. Jorjadze, V. Viasnoff, and J. Brujic. Biomimetic emulsions reveal the effect of mechanical forces on cell-cell adhesion. *Proceedings of the National Academy of Sciences*, 109(25):9839–9844, June 2012. ISSN 0027-8424, 1091-6490. doi: 10.1073/pnas.1201499109.
50. Yinghao Wu, Jeremie Vendome, Lawrence Shapiro, Avinoam Ben-Shaul, and Barry Honig. Transforming binding affinities from three dimensions to two with application to cadherin clustering. *Nature*, 475(7357):510–513, July 2011. ISSN 0028-0836, 1476-4687. doi: 10.1038/nature10183.
51. Sam Meyer, Chaoming Song, Yuliang Jin, Kun Wang, and Hernán A. Makse. Jamming in two-dimensional packings. *Physica A: Statistical Mechanics and its Applications*, 389(22): 5137–5144, November 2010. ISSN 03784371. doi: 10.1016/j.physa.2010.07.030.
52. Pierre-Olivier Strale, Laurence Duchesne, Grégoire Peyret, Lorraine Montel, Thao Nguyen, Evelyn Png, Robert Tampé, Sergey Troyanovsky, Sylvie Hénon, Benoit Ladoux, and René-Marc Mège. The formation of ordered nanoclusters controls cadherin anchoring to actin and cell–cell contact fluidity. *J Cell Biol*, 210(2):333–346, July 2015. ISSN 0021-9525, 1540-8140. doi: 10.1083/jcb.201410111.
53. H M Princen. Rheology of Foams and Highly Concentrated Emulsions. *Journal of Colloid and Interface Science*, 91(1):16, 1983.
54. K. A. Newhall, L. L. Pontani, I. Jorjadze, S. Hilgenfeldt, and J. Brujic. Size-Topology Relations in Packings of Grains, Emulsions, Foams, and Biological Cells. *Physical Review Letters*, 108(26):268001, June 2012. doi: 10.1103/PhysRevLett.108.268001.
55. Ivane Jorjadze, Lea-Laetitia Pontani, and Jasna Brujic. Microscopic Approach to the Nonlinear Elasticity of Compressed Emulsions. *Physical Review Letters*, 110(4):048302, January 2013. ISSN 0031-9007, 1079-7114. doi: 10.1103/PhysRevLett.110.048302.
56. Lea-Laetitia Pontani, Martin F. Haase, Izabela Raczkowska, and Jasna Brujic. Immiscible lipids control the morphology of patchy emulsions. *Soft Matter*, 9(29):7150, 2013. ISSN 1744-683X, 1744-6848. doi: 10.1039/c3sm51137e.
57. Connor J Thompson, Zhaoqian Su, Vinh H Vu, Yinghao Wu, Deborah E Leckband, and Daniel K Schwartz. Cadherin clusters stabilized by a combination of specific and nonspecific cis-interactions. *eLife*, 9:e59035, September 2020. ISSN 2050-084X. doi: 10.7554/eLife.59035.
58. Fei Wu, Prashant Kumar, Chen Lu, Ahmed El Marjou, Wu Qiu, Chwee Teck Lim, Jean Paul Thiery, and Ruchuan Liu. Homophilic interaction and deformation of e-cadherin and cadherin 7 probed by single molecule force spectroscopy. *Arch. Biochem. Biophys.*, 587:38–47, December 2015.
59. Amy Wang, Alexander R Dunn, and William I Weis. Mechanism of the cadherin-catenin f-actin catch bond interaction. *Elife*, 11, August 2022.
60. Bryan T Marshall, Mian Long, James W Piper, Tadayuki Yago, Rodger P McEver, and Cheng Zhu. Direct observation of catch bonds involving cell-adhesion molecules. *Nature*, 423 (6936):190–193, 2003.
61. Soonjin Hong, Regina B Troyanovsky, and Sergey M Troyanovsky. Cadherin exits the junction by switching its adhesive bond. *J. Cell Biol.*, 192(6):1073–1083, March 2011.
62. Ramesh Koirala, Andrew Vae Priest, Chi-Fu Yen, Joleen S Cheah, Willem-Jan Pannekoek, Martijn Gloerich, Soichiro Yamada, and Sanjeevi Sivasankar. Inside-out regulation of e-cadherin conformation and adhesion. *Proc. Natl. Acad. Sci. U. S. A.*, 118(30):e2104090118, July 2021.

Supplementary Data

1 Experimental Supplement

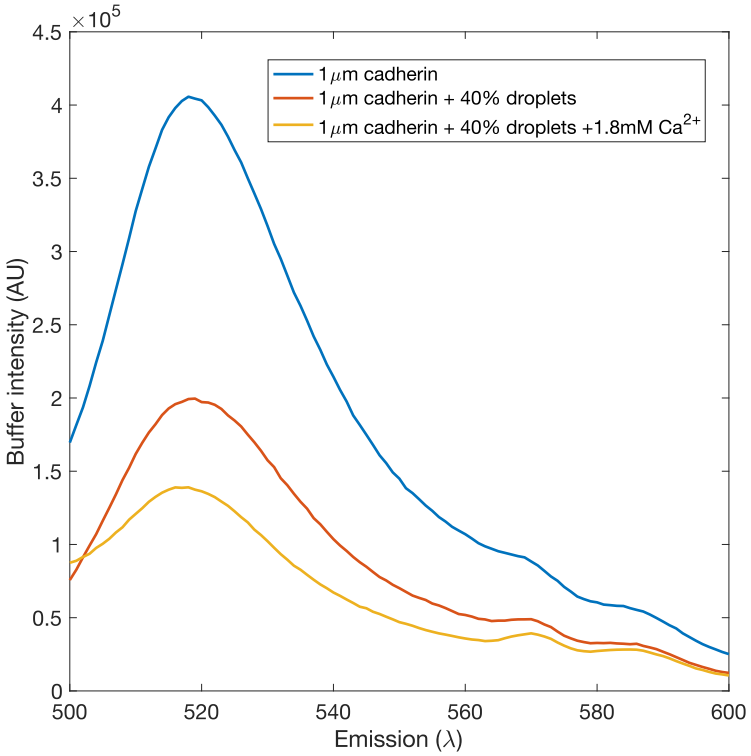

Figure S1: Fluorescence intensity of binding buffer containing cadherins. We experimentally measured the density of cadherins on the droplet surface at droplet saturation. The fluorescence intensity of $50\mu l$ a solution of $1\mu M$ E-cadherin, containing 3×10^{13} molecules was measured through a fluorimeter (Horiba-PTI QM-400 Fluorescent spectrometer). Upon adding droplets at 40% volume fraction and 1.8mM calcium, we observed a 62% loss in fluorescence intensity of the 1uM cadherin solution. This loss of intensity from the bulk solution indicated that approximately 1.8×10^{13} cadherin molecules migrated from the bulk solution on to the droplets. We estimated the droplet density to be about $3.2 \times 10^4/\mu l$, corresponding to a total droplet count of about 1.6×10^6 in a $50\mu l$ sample. Therefore, there were approximately 1.2×10^7 cadherin molecules per droplet. For a droplet of radius $10\mu m$, the surface area is $1256\mu m^2$. The density of cadherins at saturation is approximately $9.3 \times 10^3 \mu m^2$. Therefore, a saturation intensity of 150 AU for WT cadherin and 120 AU for MT cadherin corresponded to a cadherin surface density of $9.3 \times 10^4 \mu m^2$

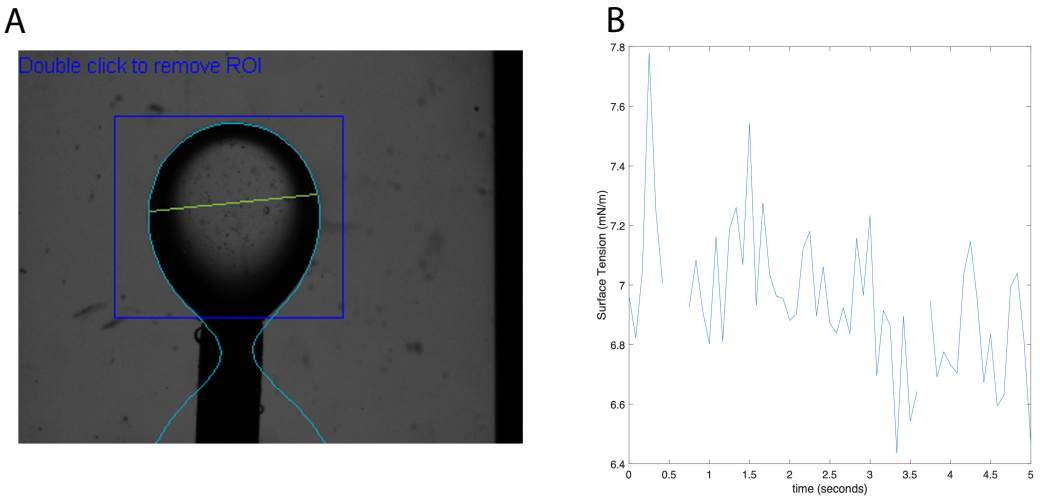

Figure S2: Experimental measurement of surface tension. (A) Surface tension is measured optically using the pendant drop method. The oil phase is injected through a hooked needle. The shape of this oil drop is determined by the balance of forces primarily between gravity and the oil-water interfacial tension. We use an optical tensiometer (Attension, Biolin Scientific, Gothenberg, Sweden). The device detects the image of the oil droplet in water, measures its size and radius R_0, and the droplet's tangent angle ϕ. Through this we obtain an estimate of the oil-water interfacial tension. (B) The average measured surface tension is 7mN/m.

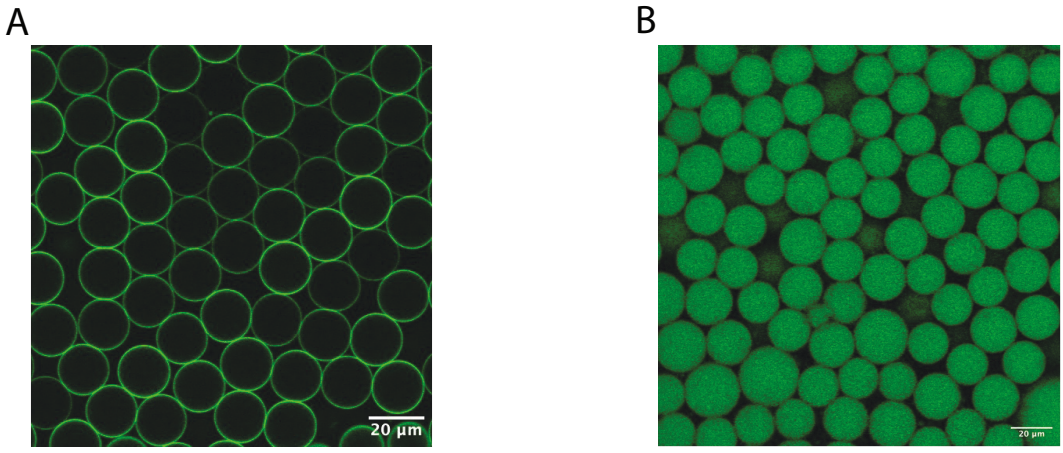

Figure S3: Negative control. (A) Cadherin-coated droplets compressed at 800g in the absence of calcium relax back to their spherical shape. Additionally, there is no recruitment of cadherins at contact points. (B) Droplets lacking cadherins but in the presence of calcium similarly relax back to their spherical shape. Droplets here are dyed with the lypophilic dye, Bodipy, for fluorescence.

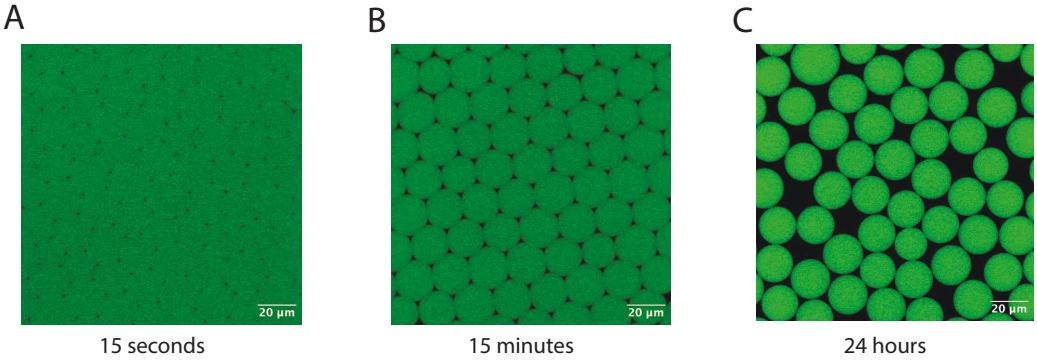

Figure S4: Droplet relaxation with time in the absence of cadherins and calcium. Panels (A-C) show how droplets dyed with Bodipy, and without cadherin adhesion relax after compressive force is remove after centrifugation over 15 seconds, 15 minutes, and 24 hours. Relaxation from full deformation to spherical begins around 15 minutes after compression is removed.

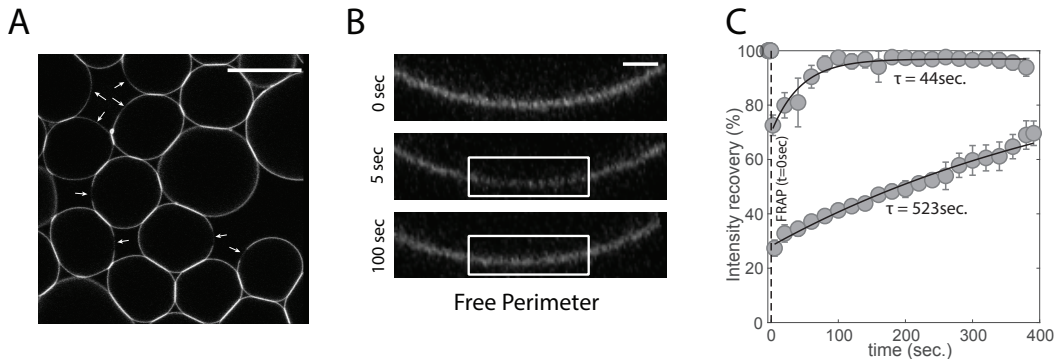

Figure S5: Analyses of fluorescence recovery at the contact-free region of droplets. (A) Overview of experiment shows the selection of contact-free regions marked by arrows for FRAP. (B) Cropped and magnified images of contact-free perimeters showing their intensity evolution of time: before bleaching at 0 seconds, 5 seconds after bleaching, and 100 seconds after bleaching. (C) Perimeter intensity as a function of time shows fluorescence recovery over time, but we observe two populations: a fast recovery time of $\tau = 44$ seconds, consistent with the diffusion of lipids in silicon oil, and a slower recovery time of $\tau = 523$ seconds, likely due to lateral inter-cadherin interactions.

2 Binding between DNA-coated droplets

The droplets used in this experiments were prepared according to[1]. Briefly, a 10 $\frac{\text{v}}{\text{v}}\%$ a monomer (Dimethoxydimethylsilane (DMDMS) and 1 mL 3-Chloropropylmethyl-dimethoxysilane (3CPMDS) were used, along with 20 $\frac{\text{v}}{\text{v}}\%$ Ammonia solution. They were polymerized until the desired size was reached.

Complementary DNA molecules with the following sequences were used (5' - 3'):

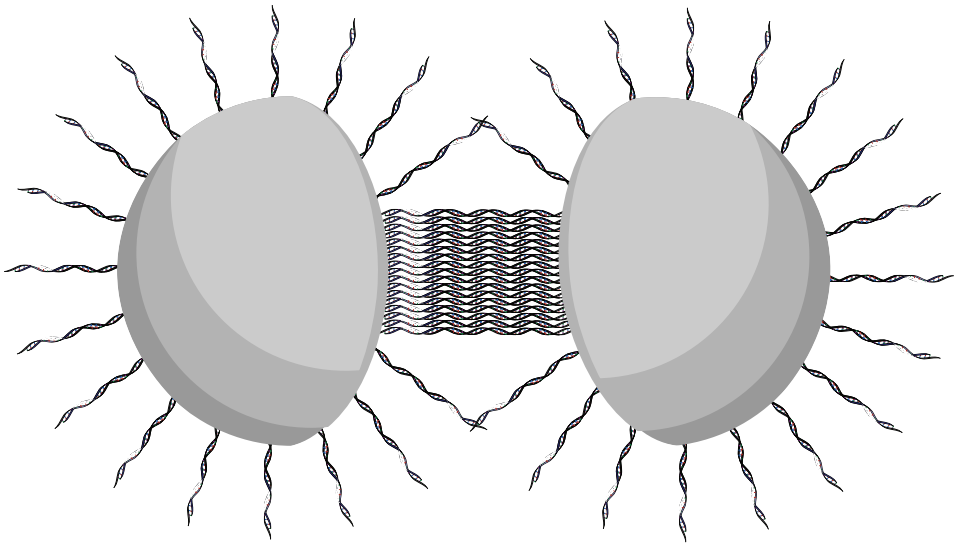

Figure S6: Schematic showing adhesion between DNA-coated droplets. Free complementary "sticky ends" (shown on individual DNA strands) bind to each other forming adhesion patches and deforming the droplet-droplet interface.

Lprime /5AzideN//iCy3/A GCA TTA CTT TCC GTC CCG AGA GAC CTA ACT GAC ACG CTT CCC ATC GCT A GA GTT CAC AAG AGT TCA CAA

Lprime/5AzideN//iCy5/A GCA TTA CTT TCC GTC CCG AGA GAC CTA ACT GAC ACG CTT CCC ATC GCT A TT GTG AAC TCT TGT GAA CTC

To prepare the droplets to be coated with the mobile DNA linkers, first the prepared droplets were washed to remove excess stabilizing SDS surrounding the droplets. This was done by filling a vial with 450 µL of 1 mM SDS. Then, 50 µL of packed droplets were procured from the prepared droplets by using an eppendorf pipette tip that had been slightly clipped to have a larger opening. This was done to ensure that droplets didn't get compressed as the packed bulk was extracted. After the packed droplets were extracted, the were washed by centrifuging the diluted vial for 10 min at 0.8 Hz. The excess solution was removed, 450 µL of 1 mM SDS was added, and the droplet solution was centrifuged for 10 min at 0.8 Hz twice more to complete the washing.

To coat the droplets with DNA linkers first, the DNA linkers and the NaCl TE Buffer (50 mM NaCl, 10 mM Tris 1 mM EDTA) were combined in 6 vials to reach a volume of 40 µL to be combined later with 10 µL of droplets to reach the following concentrations: one for the L′ DNA at final concentration 20 nM to remain constant between the conditions and five for the L DNA at final concentrations, 20 nM; 10 nM; 5 nM; 2 nM; 1 nM. The washed droplets shaken gently before 10 µL were pipetted into each vial over a vortex. After the droplets were added, the vial was shaken by hand for a short time, to allow the droplets to mix with the DNA more gently. After all the vials were prepared, they were placed in a rotator to incubate for approximately 2 h. After the droplets incubation time, 50 µL NaCl TE buffer + 0.1% Triton 165 was added to each of the vials to aid in removing

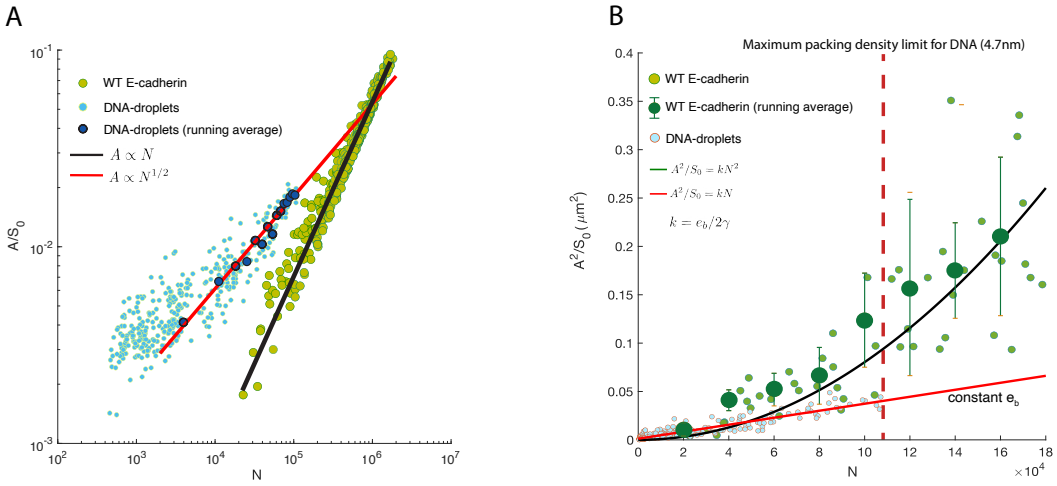

Figure S7: A log-log plot of the adhesion area (rescaled by droplet surface area S_0) as a function of binder number N in adhesions. While the area scales linearly with N (slope of 1) in the case of E-cadherin, the scaling changes to $A \propto N^{1/2}$ in the case of DNA-coated droplets. DNA binding is well captured by a simple model with a constant binding energy, in which the area grows with the density of the binders. (B) A linear plot of A^2/S_0 versus N (over a narrower range of N) confirms that the binding energy is given by the slope ($k \times 2\gamma = 1.1 k_B T$) in the case of DNA-binding. We reach a maximum packing density of DNA at $N = 110,000$ (and therefore the maximum area), when the inter-DNA distance is the known 4.7 nm packing limit (vertical dashed line). By contrast, E-cadherin data are better fit to a quadratic function, consistent with the constant crystalline density in the patches, independent of the area.

any unbound DNA left on the surface of the droplets. After this solution was added, the droplets were centrifuged at 0.8 Hz for 5 min before the excess solution was removed from each vial. 50 µL NaCl TE buffer was added to each vial before centrifuging at the same rate for the same time twice more to ensure as much of the unbound DNA was removed as possible. DNA-coated droplets formed adhesions spontaneously. They were imaged after both centrifugation without centrifugation. The adhesions patches were isolated using their intensity values and their areas measured.

3 Binding Energy Estimation

We detail in this note the computation of the deformation energy of a spherical droplet of radius R_0 into a deformed droplet with a patch of area A. We define S_0 as the initial droplet surface area, i.e: $S_0 = 4\pi R_0^2$ and we define S as the new total area of the deformed droplet. We denote by α the half summit angle of the cone whose basis is the patch of area A. The total area S is the sum of the area of the disc A and the area of the spherical cap A_s. These areas are given by

$$A = \pi(R\sin\alpha)^2, \tag{1}$$

$$A_s = \int_0^\alpha \int_0^{2\pi} d\phi R^2 \sin\theta = 2\pi(1+\cos\alpha)R^2 \tag{2}$$

Because of volume conservation, we can express R as function of α and R_0. More precisely, we have

$$R^3(\cos\alpha \sin^2\alpha + 2(1+\cos\alpha)) = 4R_0^3 \tag{3}$$

and a Taylor expansion yields $R = (1 + \frac{a^4}{16}R_0 + O(\alpha^6)$. Without approximation, the new surface S is given by

$$S = A + A_s = \pi(\sin^2\alpha + 2(1+\cos\alpha))\frac{4}{\cos\alpha \sin^2\alpha} + 2(1+\cos\alpha)^{2/3}R_0^3, \tag{4}$$

which after Taylor expansion yields

$$S = 4\pi(1 + \frac{\alpha^4}{16})R_0^2 + O(\alpha^6) \tag{5}$$

The area difference is thus given by

$$S - S_0 = \pi\frac{\alpha^4}{4}R_0^2 + O(\alpha^6). \tag{6}$$

Since we have

$$S = 4\pi(1 + \frac{\alpha^4}{16})R_0^2 + O(\alpha^6) \tag{7}$$

$$A^2 = \pi^2\alpha^4 R_0^4 + O(\alpha^6). \tag{8}$$

We can show that additional patches bring independent and similar contributions to the area increase. Considering N patches of area $A_1, ...A_N$, the total area increase is given by

$$S - S_0 = \sum_{i=1}^{N} \frac{A_i^2}{S_o}. \tag{9}$$

Finally, we estimate the binding energy by assuming a constant surface tension, γ across the droplet. For two droplets in contact, the total energy of deformation of the system will be given by

$$E_d = \gamma(S - S_0) \times 2 \tag{10}$$

$$= 2\gamma \frac{A^2}{S_0}. \tag{11}$$

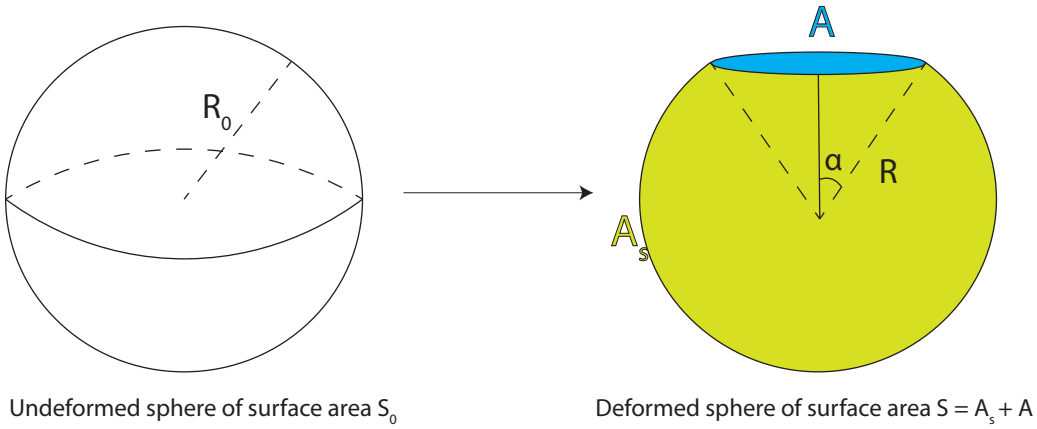

Figure S8: Schematic showing the compressed adhesion A formed when a droplet is compressed and bound to a neighbor

References

[1] McMullen, A., Hilgenfeldt, S., and Brujic, J. (2021). DNA self-organization controls valence in programmable colloid design. Proc. Natl. Acad. Sci. U. S. A., 118(46):e2112604118.